LOW-FREQUENCY OSCILLATIONS AND WEATHER REGIMES IN THE NORTHERN HEMISPHERE

R. Vautard and G. Plaut
Laboratoire de Météorologie Dynamique
Paris, France
and
Institut Non Linéaire de Nice
Nice, France

Summary: A new analysis method, multi-channel singular spectrum analysis, is used here to investigate the low-frequency dynamics in the extratropical northern hemisphere. The method is particularly efficient to extract the main oscillations, even if they are highly intermittent. We find oscillations with periods of 70 days, and 30-60 days. The spatial-temporal structure of these oscillations is presented. A few hints about the physical mechanisms explaining their existence are given. It is suggested that transients may play a crucial role in maintaining these low-frequency oscillations. Relations to weather regimes in the Atlantic are found. In particular, the European blocking is found in a particular phase of the 30-35 day Atlantic oscillation. The implications for long-range forecasting are discussed.

1. INTRODUCTION

From the dynamical systems theory, we have learnt that most forced-dissipative physical flow systems eventually evolve within a particular set of possible states, independently of the initial conditions. Although a rigorous proof of this statement can only be given for a reduced class of systems, it is generally agreed, and practically verified that, given boundary conditions, the set of possible states occurring after a long time of evolution is small, of zero Lebesgue measure and unique. In geometrical terms, the instantaneous state of a flow system is represented by a point in a high-dimensional (possibly infinite-dimensional) phase space. The time evolution is described by the trajectory of this point which tends, as time goes to infinity, to this set, called the attractor. This attractor may be a simple object, such as a point, or a periodic orbit. In these cases, the behaviour of the flow is asymptotically stationary or periodic. From the pioneering work of Lorenz (1963), we now know that aperiodic (chaotic) behaviour is to be expected in general, even when the dimension of the phase space is as low as three, and the system entirely deterministic. In the later case, the attractor is a *strange attractor* and has a complex topological structure.

Chaos, however, does not mean that the behaviour of the trajectories in phase space is random. Regularities can still be found, such as intermittent spells of regular oscillations or quasi-stationary evolution. This typically happens when weakly unstable periodic orbits or fixed points are contained in the attractor, as pictured on Fig. 1. The phase-space trajectory spends some time in the neighbourhood of the fixed point, before being ejected, and captured for a while by the periodic orbit. Lightfull examples of this behaviour are given, for instance,

in the Lorenz (1963) attractor, where two unstable fixed points compete in the attraction of the trajectories.

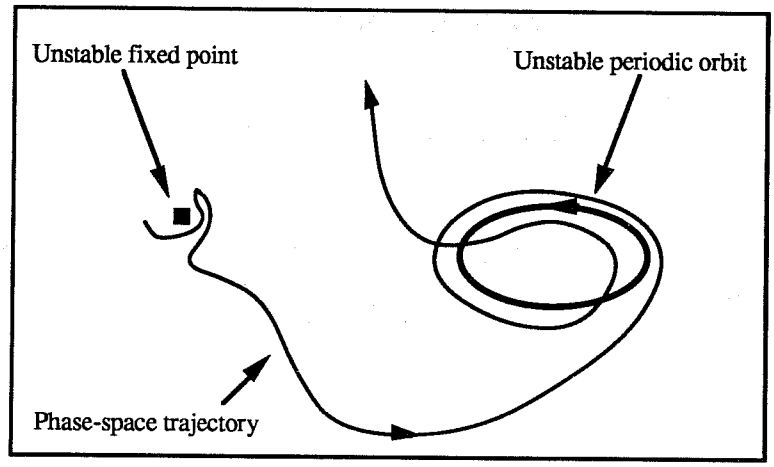

Fig. 1 Schematic picture of a phase-space trajectory vacillating between an unstable fixed point and an unstable periodic orbit.

In the context of atmospheric mid-latitude large-scale motions, quasi-stationary behaviour is observed, more generally, when some particular patterns persist beyond the synoptic time scale. The European blocking dipole is one candidate to this persistence property. This point of view was adopted first by Charney and Devore (1979), and then subsequent authors (Legras and Ghil, 1985; Itoh, 1985) who defined *weather regimes* as the stationary solutions of simplified general circulation models. Although the basic dynamical structure of the phenomenon was consistently approached by these studies, the relevance of the solution patterns to the energetics of the real baroclinic atmosphere was seriously questioned. The existence of blocking in the Charney and Devore (1979) theory is based on energy conversion from the mean zonal flow to the blocking wave through unrealistic mountain drag (at least for European blocking). Following the idea of Hoskins et al., (1983) and the numerical experiments of Shutts (1983), Vautard and Legras (1988) showed that multiple weather regimes can coexist in a reasonably realistic two-layer model with no topography.

In this model, and also as revealed by observations (Mullen, 1987), blocking is maintained by the transient baroclinic waves at the exit of a locally enhanced sheared jet. Then, the phase-space picture corresponding to a more realistic blocking would not correspond to an unstable fixed point, but rather to an unstable periodic orbit, whose projection onto the subspace spanned by the planetary waves would be a single point. Later, Vautard (1990) showed, using a 37-year long series of NMC analyses of the 700hPa height, that four large-scale patterns are likely to behave as weather regimes over the Atlantic basin. Fig. 2 shows

these patterns. The first one (BL) corresponds to the European blocking dipole, the second one (ZO) is an enhanced jet across the Atlantic, the third (GA) is a blocking high over Greenland, and the last one (AR) is characterized by a ridge over the eastern Atlantic. These were solutions of a statistical equilibration equation giving the balance of the instantaneous tendency in the neighbourhood of the solutions.

In the low-frequency range, several types of periodic activity are now well established, such as the Madden and Jullian (1971) tropical oscillation, or the extratropical 30-60 day oscillation (Weickman, 1983; Ghil and Mo, 1991). The distinction between these two oscillations is made on purpose, since their links are not clear (Dickey *et al.*, 1991). Branstator (1987) and Kushnir (1987) also showed that a wavenumber one pattern is retrogressing at high latitudes with a period of about three weeks. The intermittency of all these oscillations render them difficult to identify through classical spectral analysis. One major purpose of this paper is to present an analysis method, called *Multi-channel singular spectrum analysis*, allowing systematical identification of oscillation spells within a wide range of time scales at the same time. We focus in this paper in low-frequency oscillations (LFOs) with periods from one month to a year.

Within these time scales, large-scale patterns may act as a probabilistic environment on smaller time scales, such as baroclinic waves or even weather regimes. One particularly interesting question is whether blocking occurs at particular phases of the LFOs. This is the second point addressed in this paper. If the answer is yes, two major conclusions can be drawn. First, it would clarify partly the problem of the onset of blocking: to be triggered, blocking needs a favourable large-scale environment. Second, this answer would have an impact on blocking predictability, since an oscillation is the easiest kind of behaviour to forecast, therefore higher probability of occurrence of blocking may be predicted well in advance. It would also show that a necessary condition for a model to correctly predict blocking is that it predicts the oscillation.

In Section 2, we describe the analysis method. We show particularly that it produces data-adaptive analysing spatial-temporal filters able to isolate oscillation patterns. Then, in Section 3, the analysis of the 32-year 700hPa geopotential height data set is carried out, and the LFOs are identified. Then, a composite analysis based on the adaptively-filtered data is performed in order to estimate the spatial patterns associated to LFOs. In particular, we show the influence of LFOs onto the weather regimes identified by Vautard (1990). A short summary and discussion follows in Section 4.

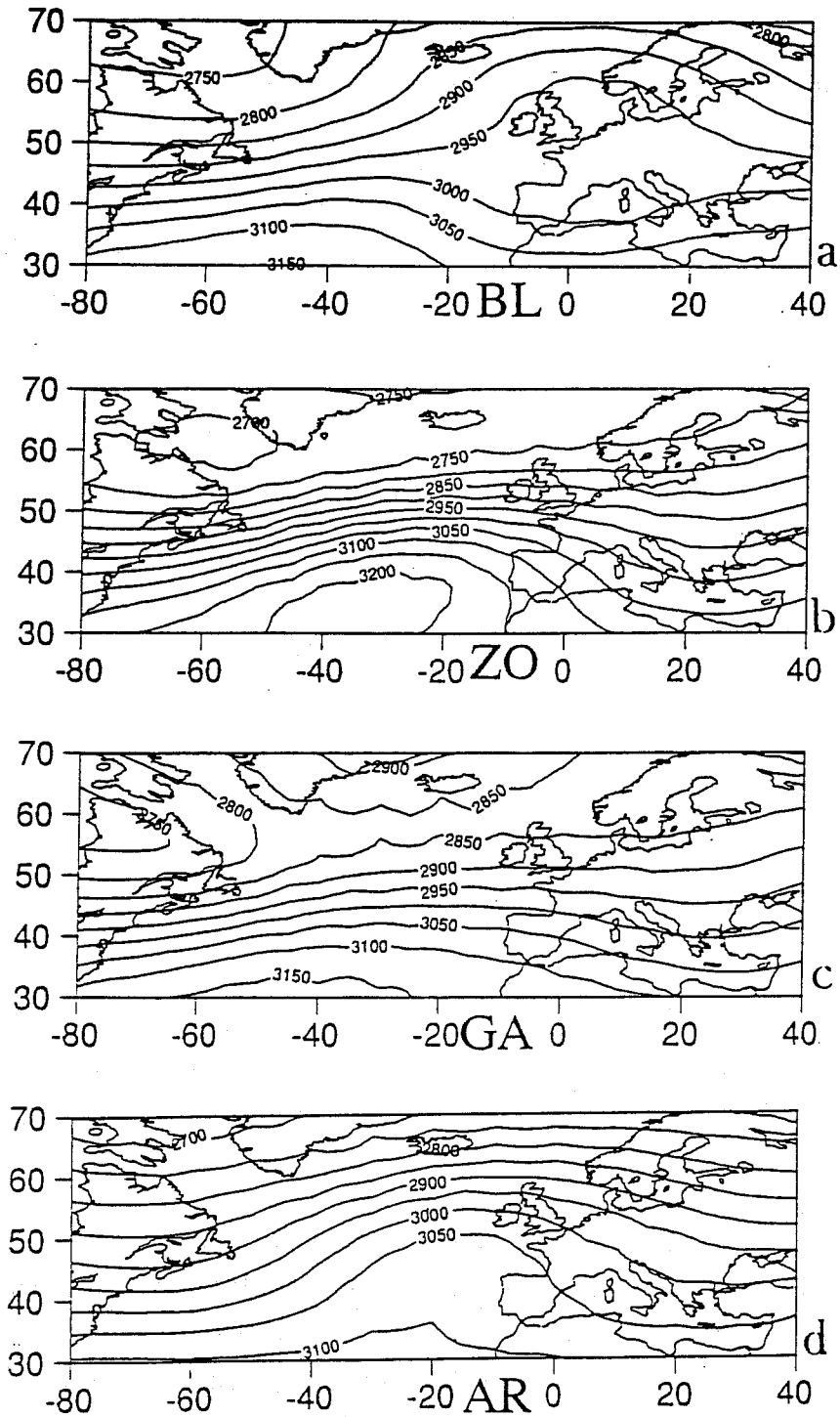

Fig. 2 Spatial patterns of the Atlantic weather regimes as identified by Vautard (1990). a) BL; b) ZO; c) GA; d) AR.

2. MULTI-CHANNEL SINGULAR SPECTRUM ANALYSIS

2.1 Theory

For a dynamical system given by a set of ordinary differential equations of the form X'=F(X), X being an L-dimensional vector, the search of unstable fixed points can be done easily, since it consists in finding the solutions of the equation F(X)=0. On the contrary, the search for unstable periodic orbits is a rather difficult task, even if the evolution equations of the system are known. This present study is observational, and therefore the governing equations are not even known. A classical method is the *Poincarré section*, in which the attractor is intersected with a given hyperplane and the trajectory traces on this subspace define a return map. The fixed points of this return map are the periodic orbits. For systems with more than three variables, this geometrical method is impossible to apply in practice, as the probability of intersecting the periodic orbit with an arbitrary hyperplane is small, unless there is a prior knowledge of the phase-space location of this orbit. The method we present here does not solve exactly this problem, but constructs, from the data, band-limited filters and associated spatial patterns.

This approach is based on a principal component analysis (PCA; Preisendorfer, 1988) of the data set, applied both in the time and in the space domain. Assume that we dispose of a data set consisting of a multi-channel time series X_{li} $1\leq i\leq N$, $1\leq l\leq L$, i representing time and l the channel number. Classical PCA gives the principal axis of this set by expanding each vector onto an orthonormal basis (E^k, $1\leq k\leq L$):

$$X_{li} = \sum_{k=1}^{M} a^k{}_i E^k{}_l , \qquad 1\leq l\leq L. \tag{2.1}$$

The projection coefficients $a^k{}_i$ are called the *principal components* (PCs), and the basis vectors E^k the *empirical orthogonal functions* (EOFs). The vectors E^k are defined as the eigenvectors of the cross-covariance matrix of the series X.

In the *single-channel singular spectrum analysis* (SSA; Broomhead and King, 1986; Vautard and Ghil, 1989; Vautard et al., 1991), a scalar series (x_i), $1\leq i\leq N$, is analysed.The SSA expansion is

$$x_{i+j} = \sum_{k=1}^{M} a^k{}_i E^k{}_j = X_{ji}, \qquad 1\leq j\leq L. \tag{2.2}$$

The analogy with PCA is made by *augmenting* the single time series x_i into the multi-channel time series $X_i = (x_{i+1}, x_{i+2}, ..., x_{i+M})$. Aside from this definition, there is no formal difference between the two expansions (2.1) and (2.2). M in the latter is called the *window length*, or *embedding dimension* - and is chosen by the user - in contradistinction with classical PCA, where M is the fixed dimension of the data vectors. The vectors E^k are the eigenvectors of the *Toeplitz matrix* of x, T_x, that contains in column j and row i the covariance of x at lag i-j.

In multi-channel SSA (M-SSA; Kimoto *et al.*, 1991), with original L-dimensional data vectors $X_{l,i}$, $1 \le l \le L$, $1 \le i \le N$, the expansion becomes

$$X_{l,i+j} = \sum_{k=1}^{LxM} a^k{}_i E^k{}_{lj}, \quad 1 \le l \le L, \; 1 \le j \le M. \tag{2.3}$$

Here, the state vector considered at time i is $(X_{1,i+1}, X_{1,i+2}, ..., X_{1,i+M}, X_{2,i+1}, ..., X_{2,i+M}, ..., X_{L,i+1}, ..., X_{L,i+M})$. M is the window length, but now the eigenvalue problem is of dimension LxM. The k-th basis vector is the eigenvector of the block-Toeplitz (LxM)x(LxM) matrix T_X containing the cross-covariance coefficients of the channels l at lags 0 to M-1:

$$T_X = \begin{pmatrix} T_{11} & T_{12} & . & . & . & T_{1L} \\ T_{21} & T_{22} & . & & & . \\ . & . & . & & & . \\ . & . & . & T_{ll'} & & . \\ . & & & . & . & T_{L-1L} \\ T_{L1} & . & . & T_{LL-1} & T_{LL} & \end{pmatrix} \tag{2.4}$$

where $T_{ll'}$ is the MxM cross-covariance Toeplitz matrix between channel l and channel l'.

The three expansions (2.1)-(2.3) are all applications of the general Karhunen-Loève bi-orthogonal expansion, and are most often used in signal processing for information compression and signal-to-noise ratio enhancement. Usually, the eigenvalues λ_k of the symmetric, nonnegative covariance matrix of the problem are sorted in descending order. The orthogonality in both time (zero cross-covariance of two different PCs at lag 0) and "space" (orthogonality of the EOFs) imply in particular that λ_k is the variance of the k-th PC. Truncating the sum in Eq. (2.1) at an order $p < M$ reduces the information to the first p principal components, instead of the M initial components. This truncation is done, in PCA, in an optimal way : the first p principal directions describe the largest fraction of the total variance that one can obtain using a projection onto p orthogonal vectors.

SSA was first introduced in nonlinear dynamics by Broomhead and King (1986), who were motivated by the reconstruction of attractors from single time series. Later, Vautard and Ghil (1989) and Vautard *et al.* (1991) showed that the SSA expansion has particular properties that make it a powerful analysis tool, and applied these to a set of paleoclimatic time series. One of the main points in these papers was that the near-equality of a pair of eigenvalues is associated with periodic activity in the signal. In contradistinction from classical spectral analysis, where the basis functions are prescribed sines and cosines, single-channel SSA can easily and automatically localize in time intermittent oscillation spells.

Since then, single-channel SSA has been applied to various geophysical data sets. Rasmusson *et al.* (1990) showed that the irregular ENSO phenomenon in the coupled ocean-atmosphere system contains a rather regular quasi-biennal signal modulated by a lower-frequency, less regular 4-5 year oscillation. Ghil and Vautard (1991) applied SSA to a 135-year long global surface temperature time series and found evidence of interannual and interdecadal oscillations. Ghil and Mo (1991) gave a comprehensive description of intraseasonal oscillations in the tropical and extratropical atmosphere.

M-SSA is then a natural extension of both PCA and SSA and has their complementary properties. It is formally equivalent to the extended EOF analysis of Weare and Nasstrom (1982), but is looked here from a different viewpoint. Kimoto *et al.* (1991) applied M-SSA to hemispheric 700hPa height maps, and focused on the three-dimensional weather pattern associated with the 30-60 days extratropical oscillation. Here, we want to give an insight on the various LFOs, using the same data, with different time scales, and their relation to weather regimes. Before, let us recall the some important properties which will help interpretmion of the results. All these properties are derived from the single-channel case, for which the reader is referred to Vautard et al. (1991) for further details.

When applied to a series of maps, for which each channel represent a grid point, PCA gives eigenvectors which are themselves maps with no definite sign or amplitude. For M-SSA, the EOFs are *time sequences* (of length M) of maps describing a travelling (or stationary) patterns. We shall call them spatial-temporal EOFs (ST-EOFs, hereafter). Equivalently, eigenvectors can be viewed as M-long time sequences in each channel. Like SSA, the crucial property of M-SSA lies in the fact that when (i) two eigenvalues are nearly equal and (ii) the two corresponding time sequences described by the EOFs are *in quadrature*, then there is in the series an oscillation whose period is the same as the period of the EOFs themselves and whose spatial pattern is the same as the one of the EOF. This correspondence can be understood with the following argument: Let us consider a portion of the series of

length M, starting at time i+1, ending at time i+M, and let us consider a component *k*. Over the portion under consideration, the expansion (2.3), combined with the orthogonality properties of the ST-EOFs would show, after a few lines of algebra, that the PC a^k_i is the value of the coefficient a which minimises the quantity

$$Q_i(a) = \sum_{j=1}^{M} \sum_{l=1}^{L} (X_{li+j} - aE^k_{lj})^2 \quad . \tag{2.5}$$

Therefore, a^k_i is the coefficient realising the least-square fit of the k-th EOF onto the original multi-channel series. Since λ_k is the variance of the *k*-th PC a_k, the spatial-temporal pattern of the k-th EOF must be recognised in the data as a dominant pattern if λ_k is relatively large. When, moreover, conditions (i) and (ii) are satisfied, for components *k* and *k*+1, the least-square fit property (2.5) remaining valid with two coefficients, a dominant oscillation stands in the signal, and has the same spatial-temporal behaviour as the corresponding EOFs.

M-SSA also provides a useful way of extracting components with different characteristics from the signal. Indeed, the sum in the right hand side of Eq. (2.3), restricted to one or several terms, represents the part of the signal behaving as the corresponding EOFs. For instance, when data are perturbed by white noise, the tail of the eigenvalue spectrum saturates at the noise variance value (Broomhead and King, 1986). The restriction made only on components of lower order provides an efficient noise reduction algorithm (Pike *et al.*, 1984; Vautard et al., 1991). The problem of reconstruction of some components is, in fact, somewhat more complex. Indeed, the individual terms of (2.3) depend on index *j*, varying from 1 to M. Therefore, there might be M ways of reconstructing several components, which do not give, in general, the same result. Vautard et al. (1991) showed that the average over these M reconstrucion estimates is optimal in some least-square sense. We define therefore the *k*-th *reconstructed component* (RC, hereafter), or *reconstruction of the k-th component,* at time *i*, and for channel *l*, by the formulæ

$$X^k_{li} = \frac{1}{M} \sum_{j=1}^{M} a^k_{i-j} E^k_{lj} \ , \qquad \text{when} \quad M \le i \le N-M+1, \tag{2.6a}$$

$$X^k_{li} = \frac{1}{i} \sum_{j=1}^{i} a^k_{i-j} E^k_{lj} \ , \qquad \text{when} \quad 1 \le i \le M-1, \tag{2.6b}$$

$$X^k_{li} = \frac{1}{N-i+1} \sum_{j=i-N+M}^{M} a^k_{i-j} E^k_{lj} \ , \qquad \text{when } N-M+2 \le i \le N. \tag{2.6c}$$

Eq. (2.6a) is the general case, and the distinction is made when time i is close to the ends of the series, since the average cannot run on all the terms. Unlike PCs, which are scalar series, RCs are multi-channel series, representing the part of the original signal corresponding to the associated eigenelements. RCs have additive properties, and the enormous advantage that the original signal is *exactly* the sum of all the RCs:

$$X_{li} = \sum_{k=1}^{LxM} X^k{}_{li} \quad . \tag{2.7}$$

A reconstructed oscillation given by the pair (k, k+1) of eigenelements is then simply the sum $X^k{}_{li} + X^{k+1}{}_{li}$. Ghil and Mo (1991) defined a statistical test based upon assumption (i) and (ii) in order to identify pairs of eigenelements associated with oscillations, which we shall use here.

From the spectral point of view, PCs and RCs keep similar properties as for the single-channel case. Denoting by $P_{ll}(f)$ the power spectrum of the series in channel l, and by $P_{ll'}(f)$ the cross-spectrum of two channels l and l', the power spectrum $P^k(f)$ of the k-th PC writes

$$P^k(f) = \sum_{l,l'=1}^{M} P_{ll'}(f)\Phi^k{}_l(f)\,\overline{\Phi^k{}_{l'}(f)} \quad , \tag{2.8}$$

where

$$\Phi^k{}_l(f) = \sum_{j=1}^{M} E^k{}_{lj} e^{2i\pi f} \tag{2.9}$$

is the Fourier transform of the k-th ST-EOF in channel l. Unlike for single-channel SSA, PCs cannot be interpreted directly as filtered versions of the original series, since the coherence between all the channels is taken into account in the transform. Nonetheless, a similar global property occurs: if P(f) is the total spectrum of the series, i.e.

$$P(f) = \sum_{l=1}^{L} P_{ll}(f) \quad , \tag{2.10}$$

the sum of the spectra of individual PCs is proportional to P(f), i.e.

$$P(f) = \frac{1}{M} \sum_{k=1}^{LxM} P^k(f) \quad . \tag{2.11}$$

Eq. (2.11) is particularly interesting to identify the relative contribution of one or a pair of components in different frequency bands. A major difference between scalar series and multi-channel series is that several spatial patterns may respond in the same frequency band. Therefore, a strong advantage of M-SSA with respect to any other spectral method is to distinguish them.

There are subtle links between SSA or M-SSA and maximum entropy (ME) spectral estimates. In the single-channel case, for instance, the same Toeplitz matrix is used for diagonalisation and estimating coefficients of an M-1-order autoregressive model. Penland *et al.* (1991) gave a first insight into these links. Vautard et al. (1991) developed a ME spectral approach fully-consistent with SSA. For M-SSA, the problem is more complex, as we are dealing with multi-channel ME autoregressive models. Still, the problem can be handled (Plaut and Vautard, 1991). A multi-channel autoregressive model is built

$$Y_i = A_1 Y_{i-1} + A_2 Y_{i-2} + \ldots + A_{M-1} Y_{i-M+1} + W_i \quad , \qquad (2.12)$$

where Y_i is the "state" vector of dimension L at time *i*, and A_j are regression matrices, instead of regression coefficients in the single-channel case, and W is a white noise process. This model is built in such a way that the stochastic process Y has the same lagged cross-covariance matrix T_Y as T_X. Under these assumptions, the channels of Y has ME power spectra and cross-spectra taking the form of inverses of complex polynomials of the variable $\zeta=e^{2i\pi f}$. Then PCs have power spectra taking the form of complex rational fractions of the variable ζ. All the poles of these meromorphic functions lie inside the unit circle, due to the stationarity of the time series. All these ME spectral estimates satisfy the property given by Eq. (2.11). Spectra shown in Section 3 are calculated in this way. A major weakness of ME spectral estimates is their lack of statistical significance estimators. In practice, here, we will assess statistical significance by checking the stability of the results when the parameters of the method are varied.

A major problem, when using SSA or M-SSA, is the choice of the window length M. Generally, the larger the window length, the sharper the spectral resolution. With large window lengths, one is able to distinguish between two close spectral peaks. The price to pay is a poorer temporal localisation of the intermittent oscillation spells. When the data series is short, one is also faced with the problem of statistical significance. The larger M, the poorer the statistical significance. With the long data set we will use, this latter problem will not occur. Vautard et al. (1991) showed that the optimal window length M would be the average *life time* of the oscillation to be studied. Since this cannot be determined a priori, one is left

with a typical rule: an analysis with window length M resolves oscillations with periods in the range (M/5, M). Oscillations with smaller periods will be resolved but badly localised in time through reconstruction (too small amplitudes in the oscillation spells and too large amplitudes outside), whereas larger periods will hardly be distinguished from one another. However, as we shall see for the annual cycle, when *lines* are present in the spectrum, corresponding to permanent oscillations, their identification is always achieved even with windows shorter than the period.

2.2 Experimental design

M-SSA is applied on geopotential height fields at 700 hPa which were provided to us by K. Mo at the National Meteorological Center. The maps are defined on the NMC diamond grid, consisting of two shifted 10°x10° grids. In order to avoid erroneous data, the grid is restricted to the latitude band (30°N to 80°N). We analyse data over three domains; the whole northern hemisphere (NH), consisting in 396 grid points; a domain covering the north Atlantic and Europe (ATL, 30°N to 70°N and 80°W to 40°E), which was also used to define the Atlantic weather regimes (Vautard, 1990); the Pacific domain (PAC), for which the window extends from 30°N to 70°N again, and from 140°E to 100°W. The local domains include 113 grid points. 32 years, starting on 1 may 1954 and ending on 30 april 1986 are analysed. No prior time filtering is applied in order not to bias the analysis.

The main numerical difficulty lies in the fact that M-SSA diagonalises big matrices. For the NH grid, a window length of, say, M=100 days would lead to diagonalising a matrix of size 39600. Moreover, we are mostly interested here in low-frequency, or equivalently large-scale phenomena. Therefore, we first apply a classical PCA in order to compress the information within fewer directions. PCA gives 396 spatial EOFs (s-EOFs) for the NH experiment, and 113 s-EOFs for the local analysis. Among these EOFs, some of them are of particularly large scale and evolve with long time scales. In order to objectively extract these spatial components, we estimate the power spectra of all the spatial PCs (s-PCs). These spectra are separated into low-frequencies (periods longer than a week (7 days), and high frequencies (periods lower than 7 days). NH PCs for which more than 85% of the variance is confined within the low frequencies are kept as the low-frequency (or equivalently large-scale) PCs. The same procedure of extraction is applied for the ATL and PAC PCs, but with a criterion of 75%. These numbers were in fact chosen in such a way that no baroclinic wavetrains are retained in the large-scales variables. This leads to retaining PCs #1 to 13, and 16 to 17 for the NH domain, PCs #1 to 10 for the ATL domain, and PCs #1 to 10 and 12 to 14 for the PAC domain. The s-PCs are scalar time series. M-SSA is applied to these large-

scale variables defining the L channels of Section 2.1. For NH, we have L=15, for PAC L=12, and for ATL L=10.

A first series of experiments is performed with a window length of 200 days with these data sets. In order to avoid computer memory problems, a sampling rate of 5 days is taken. Then, M=40, and the matrice sizes are 600 for NH, 400 for ATL and 480 for PAC. As mentioned in Section 2.1, this window length should successfully resolve and localise intermittent oscillations with periods in the range 40-200 days. In order to analyse better the variability from two weeks to a season, a second series of experiments is performed with a window length of 100 days and a sampling rate of 2 days. For this second series of experiments, we remove the long-term regular behaviour by using the adaptive reconstruction filters directly provided by the first series of experiments. More precisely, using Eq. (2.7), the original multichannel series X is splitted into

$$X = Y + Z \quad , \tag{2.13}$$

where

$$Y_{li} = \sum_{k=1}^{P} X^k{}_{li} \tag{2.14a}$$

and

$$Z_{li} = \sum_{k=P+1}^{MxL} X^k{}_{li} \quad . \tag{2.14a}$$

In Eqs. (2.14), P is a suitably chosen order, after which ST-EOFs start to respond with periods smaller than 60 days. Z is therefore an adaptively-filtered series which will be used in particular for studying the 30-60 days extratropical variability. The choice of P is decided after the analysis of the first experiment. We take P=9 for all domains. As we shall see in Section 3, this choice also removes adaptively the annual cycle in the series Z.

3. STRUCTURE OF THE LOW-FREQUENCY OSCILLATIONS

3.1 Results for the ATL domain

With a window of 200 days, we obtain three pairs of eigenelements associated with oscillations. The first pair (1-2) describes exclusively the annual cycle, together with the interannual variability. The spatial patterns of the ST-EOFs (not shown) are essentially uniform over the Atlantic. The annual cycle consists in a global rise or decrease of the geopotential height. Fig. 3 shows the reconstruction X^1+X^2 of channel l=1 for years 1982 to 1986. This figure shows clearly how efficient the reconstruction algorithm is in extracting

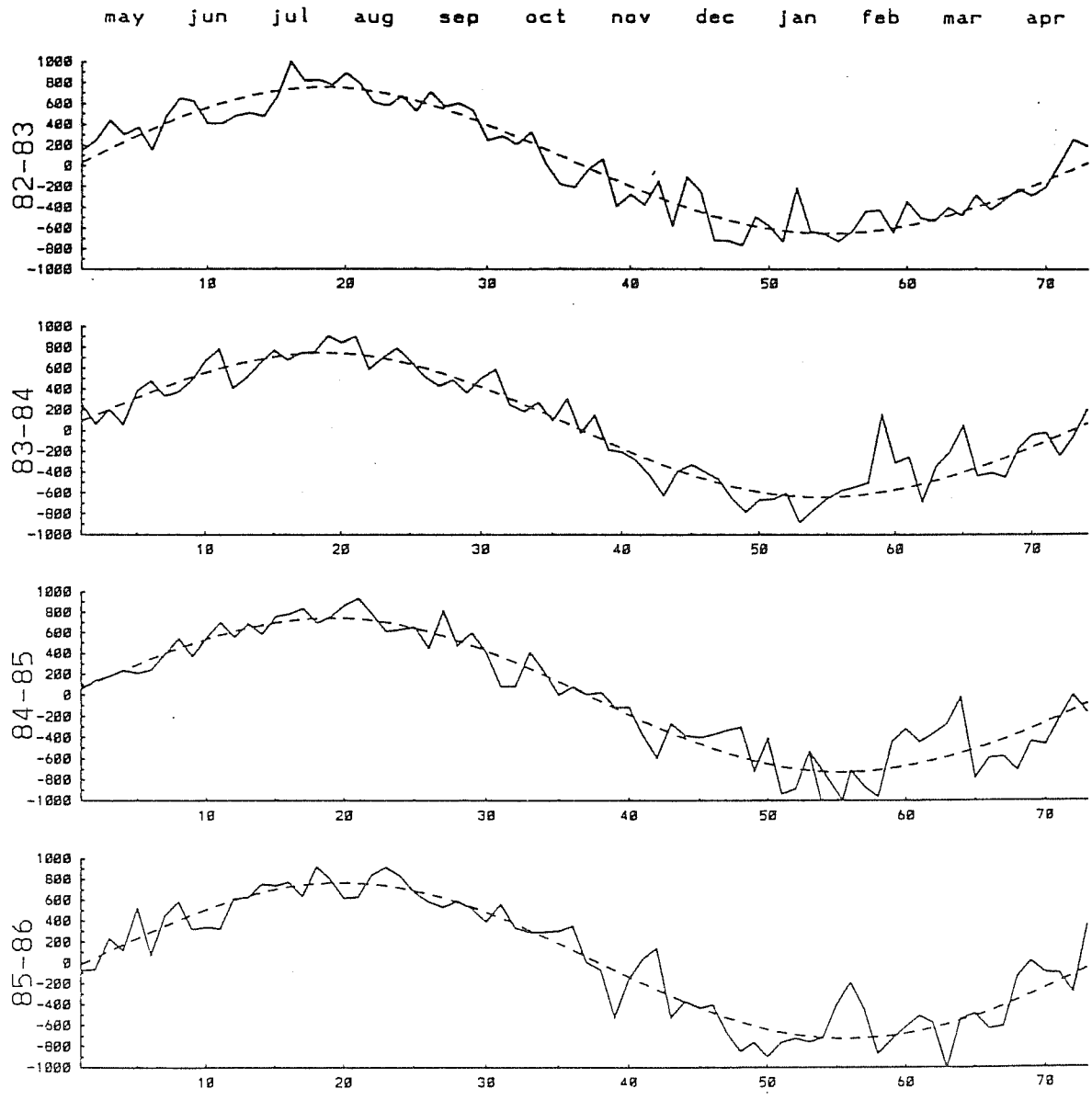

Fig. 3 Time evolution of ATL s-PC 1 for years 82-83 to 85-86 (end of the series). The solid curve represents the unfiltered s-PC, the dashed curve is the reconstruction based on components 1 and 2 (X^1+X^2) representing the annual cycle.

dominant oscillations, even at the ends of the series, where accuracy is theoretically reduced by the lower number of PC values to be averaged (see Section 2.1). Then, ST-EOFs 3 to 6 are less regular. The associated spatial patterns (not shown) still show some coherence in that they all exhibit a poleward propagation of a zonally elongated dipole across the domain. The associated fluctuations are associated with variations in the position of the Atlantic jet stream.

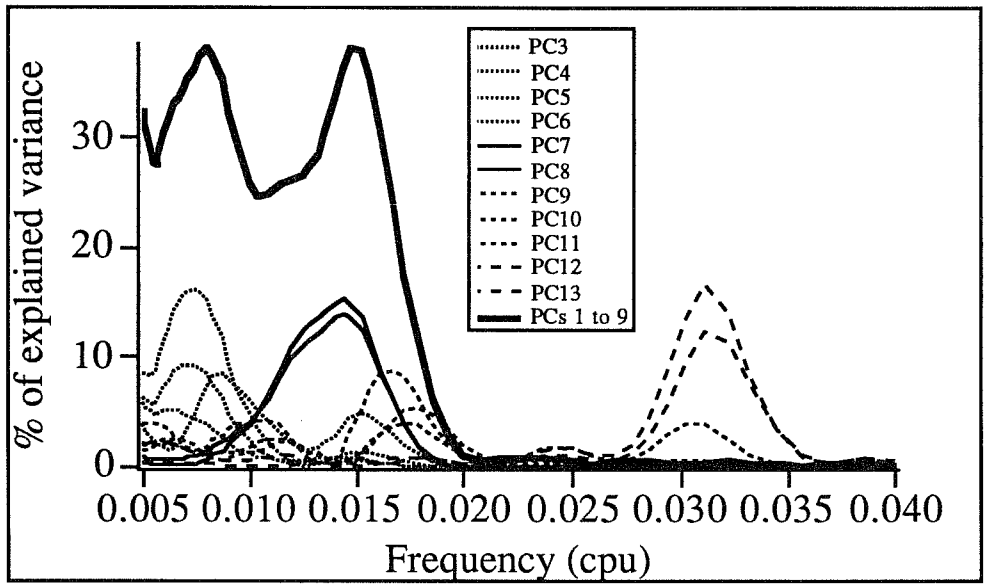

Fig. 4 Percentage of the variance explained by the ATL ST-PCs 3 to 13 (thin curves), and the *total* variance explained by the ATL ST-PCs 1 to 9, as a function of frequency. Curves are calculated from Eq. (2.15).

Fig. 4 shows the fraction

$$F^k(f) = \frac{P^k(f)}{MP(f)} \qquad (2.15)$$

of the variance explained by PCs 3 to 13, as a function of frequency. The spectra involved in Eq. (2.15) are calculated with the maximum entropy-SSA method mentioned in Section 2.1. From Fig. 4, one sees that the periods involved in ST-components 3 to 6 lie between 100 and 200 days.The second pair of eigenelements is clearly represented on Fig. 4 with components 7 and 8. Their explained variance are nearly equal at all frequencies, and peak at about 70 days. Also indicated in Fig. 4 is the fact that this oscillation explains about 30% of the total variance near 70 days. The spatial-temporal evolution of ST-EOF 7 is shown on Fig. 5, at four selected days of the 200 day sequence, with a 10 day interval between maps, so the oscillation achieves slightly less than half a complete cycle. Just as for Components 3 to 6, the oscillation consists in a poleward propagation of a zonally elongated dipole, associated with fluctuation both in position and intensity of the Atlantic jet. Note that the dominant pattern

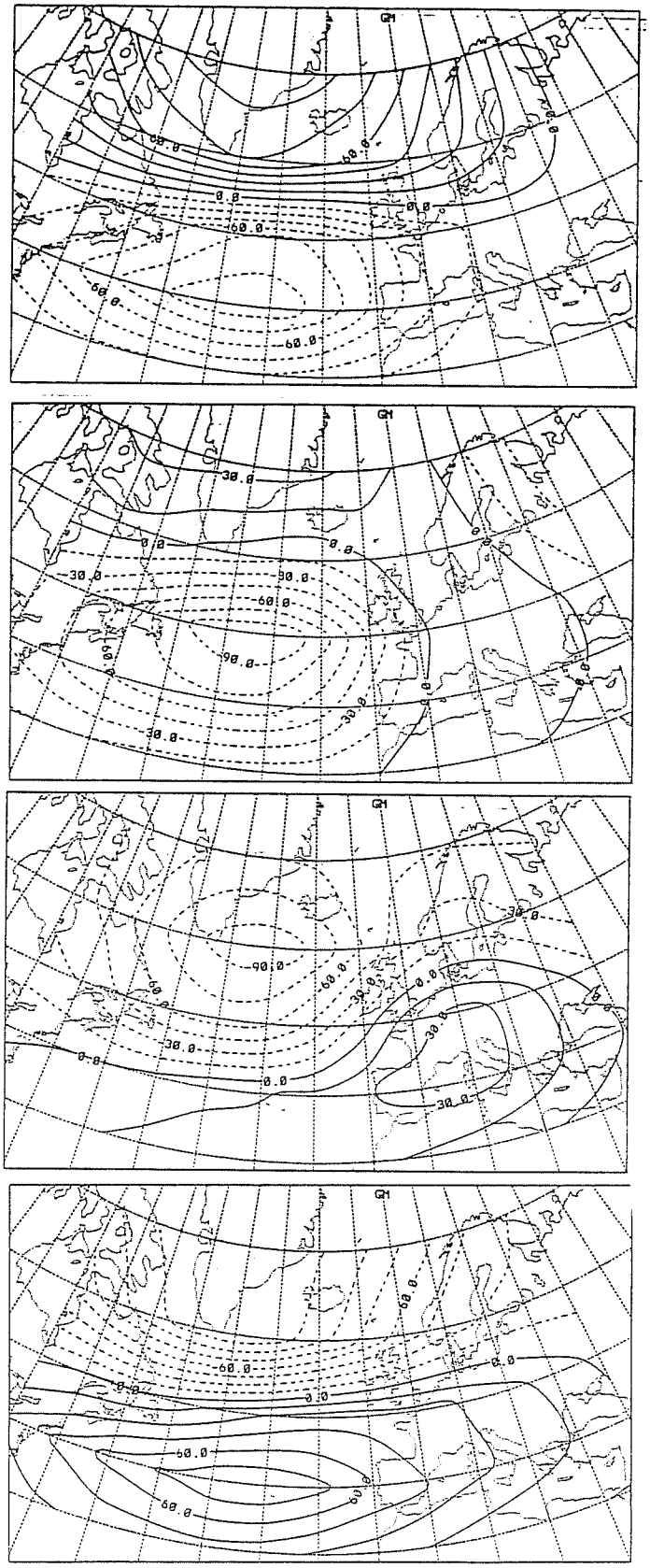

Fig. 5 Contours of the spatial patterns of the ST-EOF 7 for the ATL experiment with a window length of 200 days. The ST-EOF is 200 day long, and are represented only patterns at days 55 (a), 65 (b), 75 (c), and 85 (d). Units are arbitrary. Dashed contours correspond to negative values.

oscillating here is the now classical North Atlantic Oscillation (NAO) teleconnection pattern of Wallace and Gutzler (1981). The amplitude of the anomaly is stronger when the oscillation is in phase or in opposite phase with the NAO.

Visual inspection of the reconstructed component X^7+X^8 associated with this oscillation shows that its amplitude is usually larger in the cold season. This is, in fact, a general property of all the oscillations we will analyse here. Fig. 6 shows the projection of the reconstructed oscillation X^7+X^8 for the 1961-1962-1963 onto the plane spanned by s-EOFs 1 and 2. The amplitude of the oscillation was particularly strong during winter 61-62 (period of larger distance to the origin, on Fig. 6). The reconstructed trajectory turns anticlockwise around the origin. In order to build composite maps, we define 8 sectors separated by the straight lines on Fig. 6. Then, composites are calculated, based on all *winter* data falling within these sectors, winter being the period starting on 15 november and lasting 136 days (ending then approximately on 31 march).

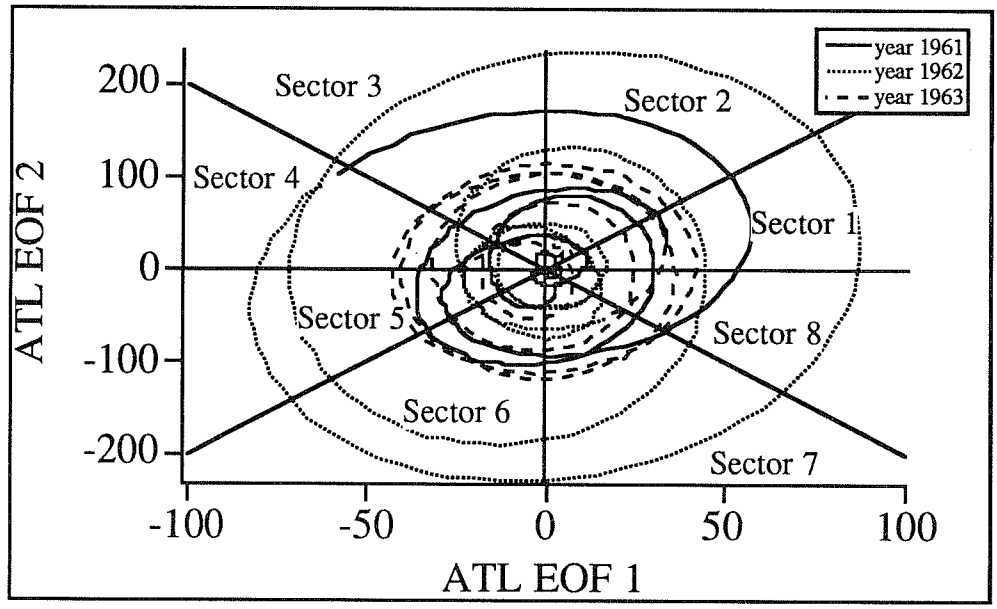

Fig. 6 Projection, onto ATL s-EOFs 1 and 2 of the 70 day oscillation reconstructed with the ST-components 7 and 8, for the selected years 1961, 1962 and 1963. The trajectory turns anticlockwise. Also shown are the sectors used for composite analysis.

The composites of raw hemispheric anomalies keyed to sectors 5 to 8 (over the lower half of Fig. 6) are shown on Fig. 7. Symmetric sectors lead to opposite anomalies. The amplitude of the winter anomalies are not small, since they reach 60 meters in sector 5, and even 70 meters in sector 2 (not shown). An important feature revealed by these composites is the development of a significant low over Siberia in sector 5, although this area is off the domain studied. No significant anomaly is found over the Pacific area. The Siberian trough

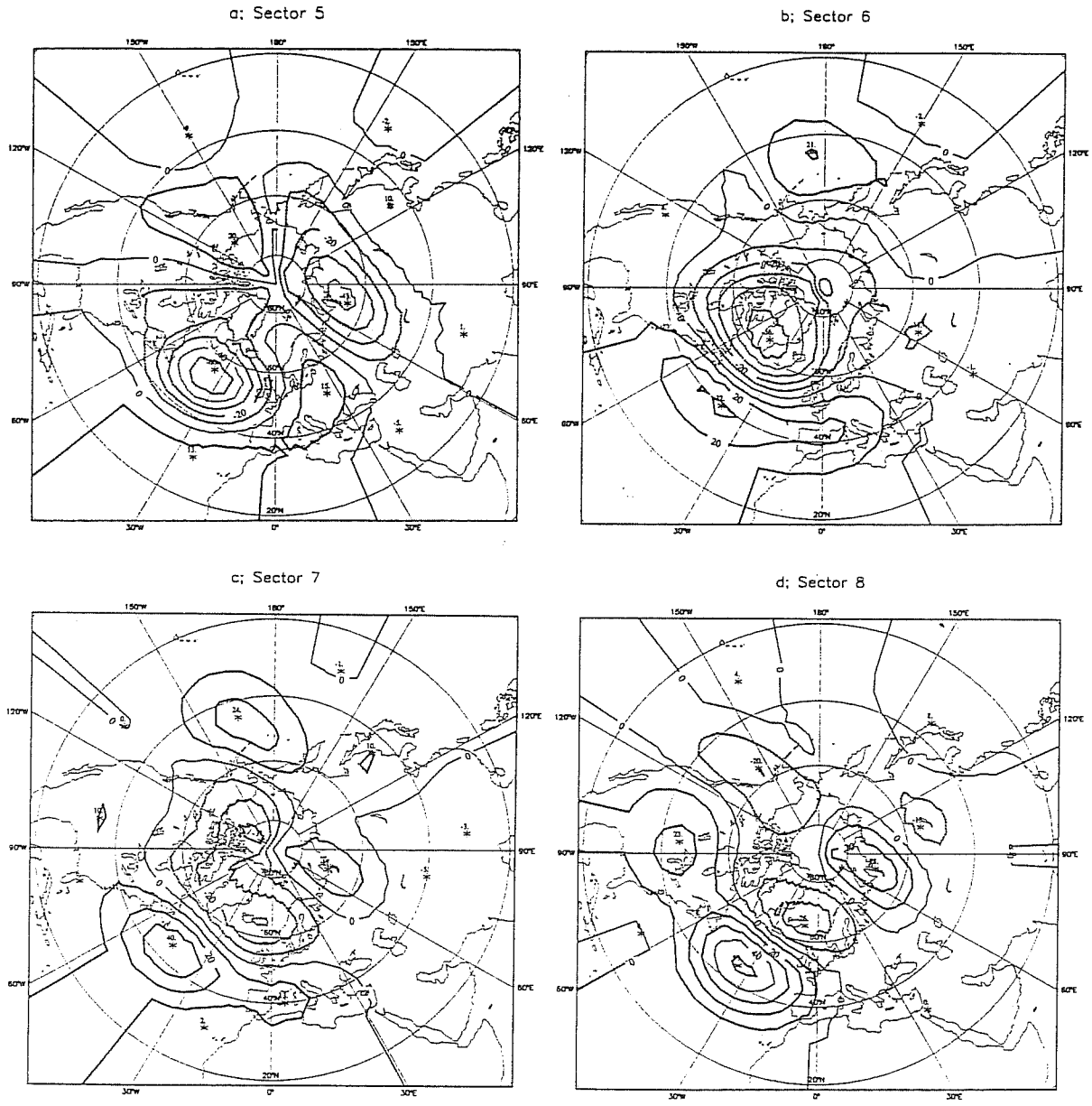

Fig. 7 Contours of the global composites of the raw 700 hPa geopotential height key to sectors 5 to 8 of the 70 day ATL oscillation. a) sector 5; b) sector 6; c) sector 7; d) sector 8.

develops when the Atlantic jet is displaced southward. No obvious interpretation of this can be drawn. During the phase corresponding to sectors 6 and 7, the Atlantic jet is intensified and slightly displaced northward, and the anomaly is restricted to the north Atlantic ocean. Such a poleward displacement of the jet could be explained by the classical poleward transport of zonal momentum by transient baroclinic waves. When the jet is intensified, transients are.overdevelopped and tend to advect the jet poleward. The opposite action takes place in the opposite phase. Such a behaviour is however only suggestive and should be taken with care, as long as a composite analysis of the action of the transients is not performed.

Components 9 to 11 are more irregular low-frequency components, and the third pair of eigenelements is found for components 12 and 13. As shown by Fig. 4, this pair is associated with a 30-35 day oscillation, explaining again about 30% of the variance in this frequency band. The spatial structure of this travelling wave will be discussed more in detail using the 100 day window. On Fig.4 is also shown the variance explained by components 1 to 9, calculated by summing up the contributions of individual PCs. It is clear that most of the variance remains unexplained, even for periods greater than 60 days. This indicates that a rather large number of large-scale patterns respond at these frequencies, and the variance cannot be represented by less than, say, 10 patterns. In fact, the rest of the variance is spread rather regularly into the remaining components ($k \geq 10$).

When RCs 1 to 9 are removed from the raw data series X, the resulting series Z, analysed with a window length of 100 days, exhibits only one very regular pair, again associated with an oscillation having a period of 30-35 days. Sector composites build in the same manner as for the 70 day oscillation, but with different coordinates, are displayed on Fig. 8. The amplitude of the anomalies again reach 50-60 meters. From sector 5 to 6, an Atlantic north-south dipole is rapidly replaced by an east-west dipole, the negative anomaly travelling westward. A positive anomaly builds up over Scandinavia, together with a small-amplitude negative anomaly southward. There is a quadrupole structure more or less clear on sector 6. The new dipole formed on phase 7 then travels westward during the next two sectors. We chose sectors in such a way that the times spent in all sectors are approximately equal. Therefore, the phases during which the anomaly propagates westward are slow phases. Note that the pattern obtained in sector 7, which is precisely a slow phase, is strongly reminiscent of the European blocking pattern.

The westward travel of blocking dipoles has already been pointed out by Rex (1950), and associated with explosive cyclogenesis by Colucci (1985). In the work of Mullen (1987), transients have a feed-back onto blocking essentially in quadrature ahead of the dipole.

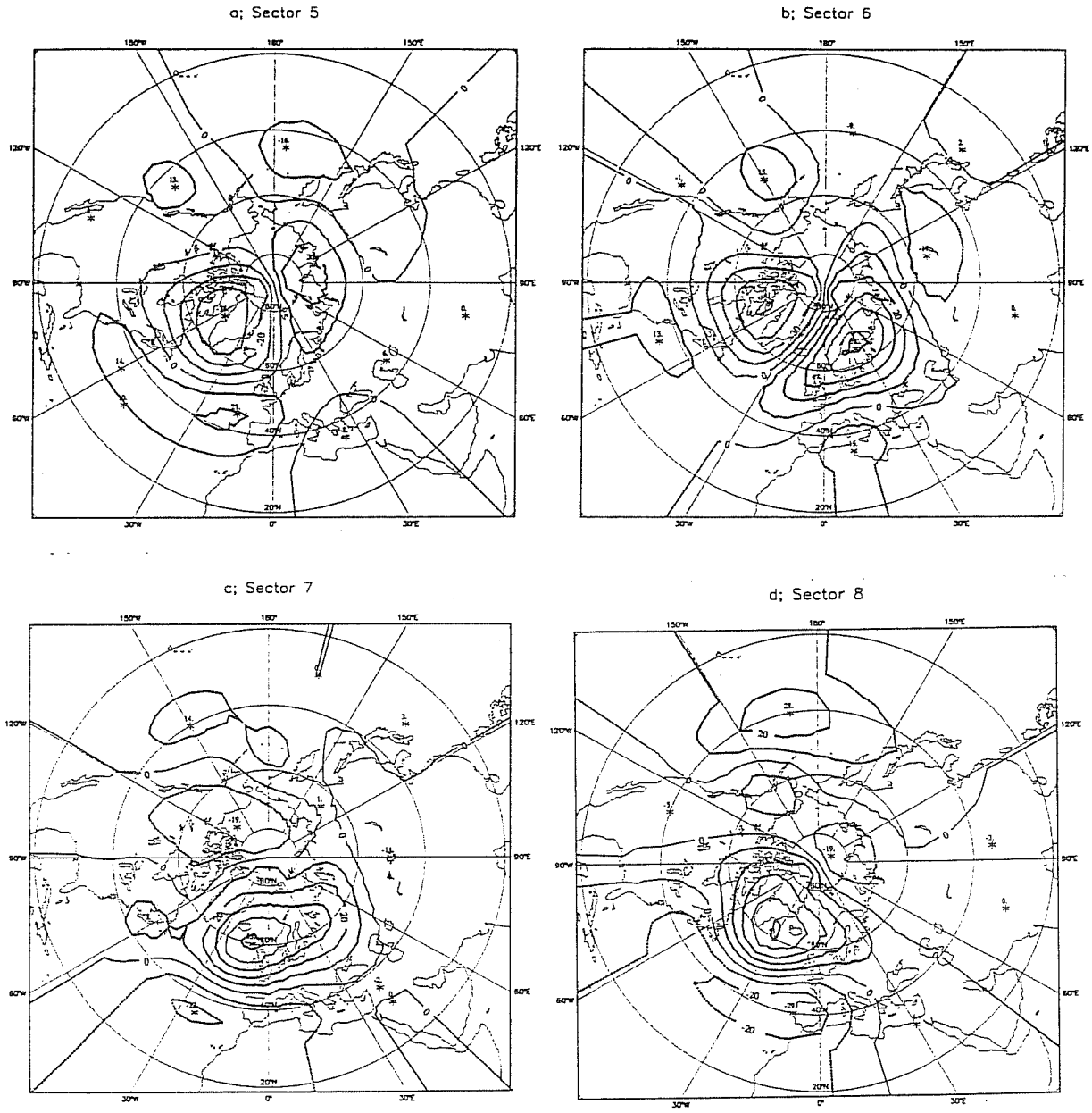

Fig. 8 Same as Fig. 7 for the ATL 30-35 day oscillation. Sectors are defined using s-PCs 2 and 4. Reconstruction is made using ST-components 1 and 2 of the 100-day window experiment.

Therefore, an excess of baroclinic activity due to a jet reinforced by the upstream part of the quadrupole would tend to advect the diffluence westward. Again, these interpretations are to be justified by a more rigourous composite analysis. The period of this oscillation is also suggestive of links with the tropical Madden and Jullian oscillation. Considerable insight in this direction has been given by Kimoto *et al.* (1991). However, as shown by Dickey *et al.*, the tropical oscillation reflected in the angular momentum is more likely to respond with a period near 50 days. Yet, the hypothesis of a coupling cannot be rejected.

3.2 Results for the PAC domain

For a window length of 200 days, the PAC area exhibits five distinct oscillations. First, as for the ATL area, the pair 1-2 explains the annual cycle. The pair 3-4 is associated with a marked harmonic of the annual cycle, with a period of 186 days. This is clear when one checks for the phase locking between these cycles. Also, the pair 6-7 is phase-locked with the annual cycle, with a period of about 120 days. This is particularly obvious if one plots the trajectory of PC#6 versus PC#1 (Fig.9). The trajectory describes roughly a Lissajoux curve. The conclusion is that this pair corresponds to the third harmonic of the annual cycle. Its spatial-temporal pattern is a standing wave showing a marked PNA.

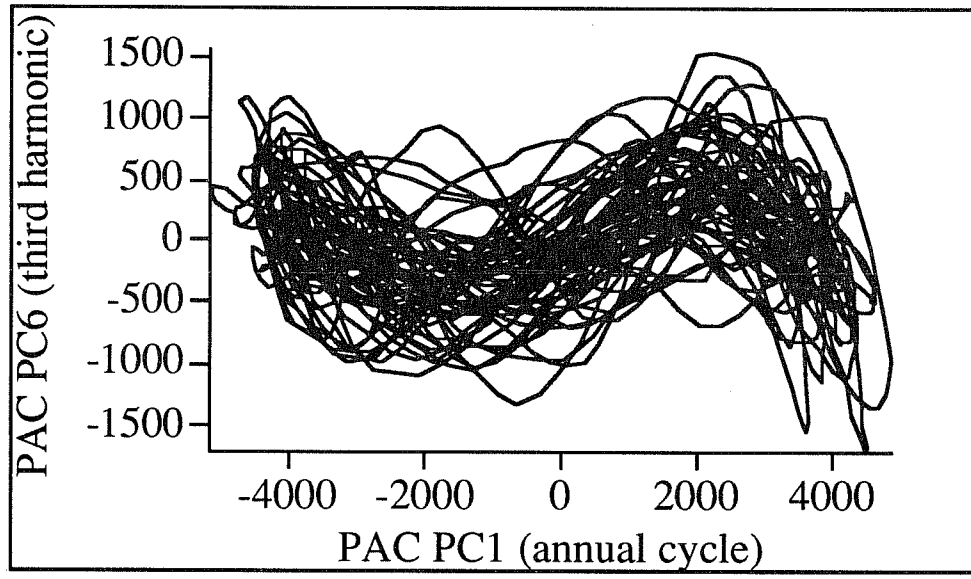

Fig. 9 Time evolution of ST-PC 6 versus ST-PC 1 for the PAC 200 day experiment. The 32 years are displayed.

Next, pair 10-11 has a dominant period of about 50 days, and pair 12-13 a dominant period of 30-35 days. These latter ones will be discussed in the second experiment. Note that no 70 day oscillation is found for the PAC domain, again suggesting that this mode is characteristic of the ATL domain. The variance explained by the oscillations (not shown) is

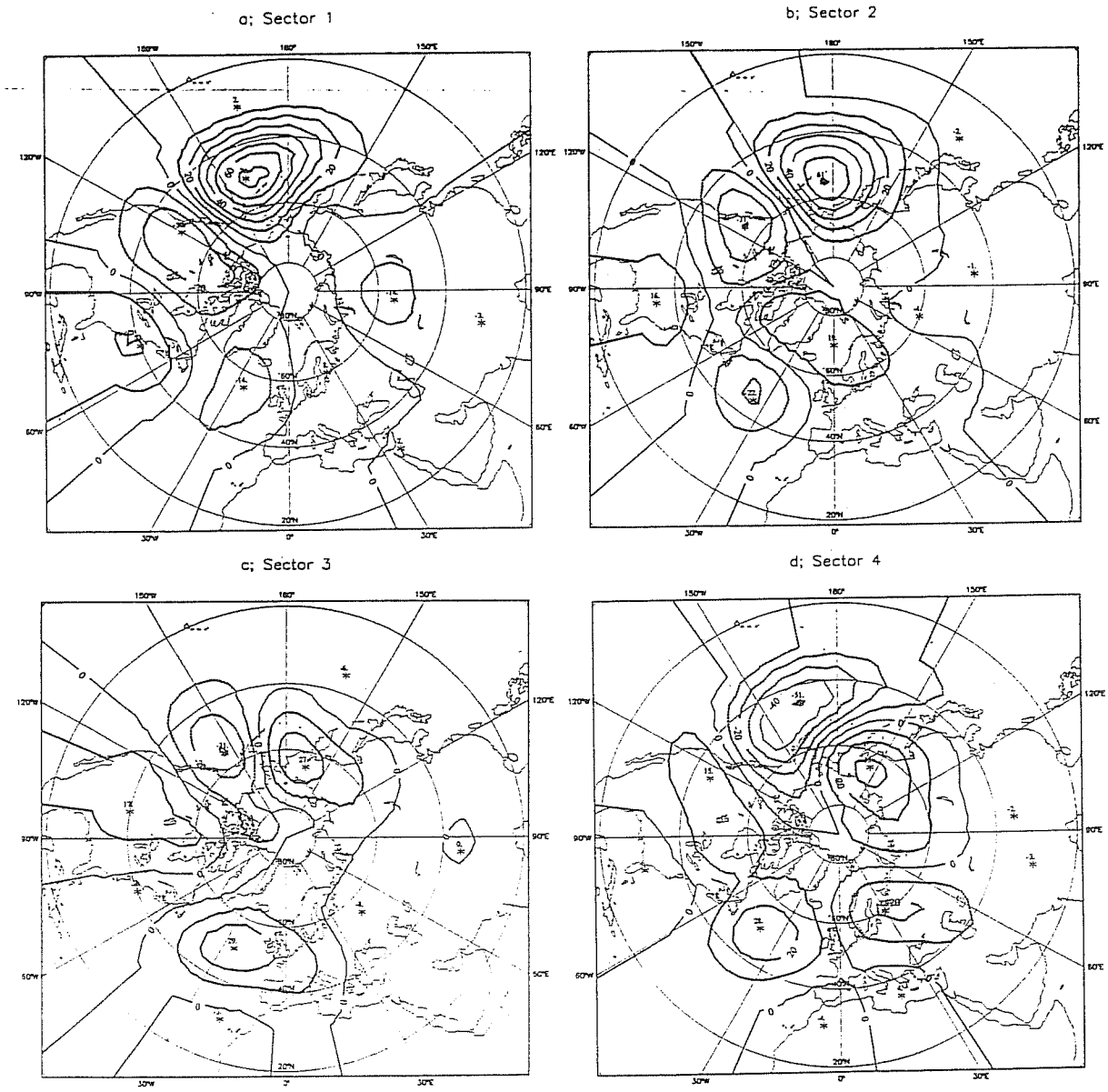

Fig. 10 Same as Fig. 7, for the four sectors 1-4 of the PAC (100 day window) 50 day oscillation (ST-components 1-2).

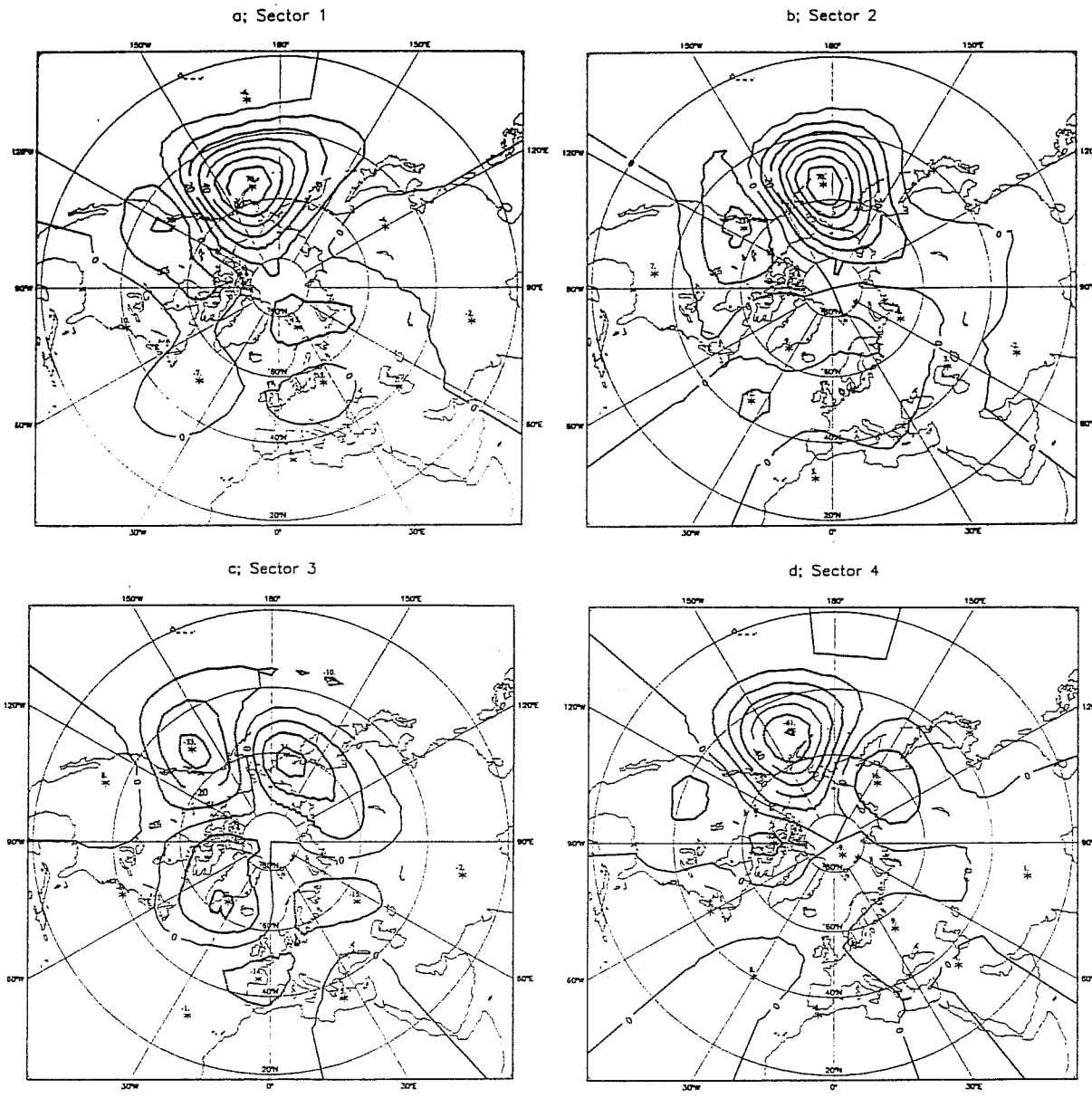

Fig. 11 Same as Fig. 7, for the four sectors 1-4 of the PAC (100 day window) 30-35 day oscillation (ST-components 3-4).

again approximately 1/3 of the total variance near their period. The variance explained by the first 9 components behaves in the same way as for the ATL case.

When a 100 day window length is considered, three major pairs stand out. The first one, pair 1-2 corresponds to a 50 day oscillation. Its spatial-temporal evolution is represented on Fig. 10, as composites done in a similar way as for the ATL experiments. A PNA pattern dominates on sectors 1 and 2, with a maximum amplitude of more than 70m in sector 1. Then, the wavetrain retrogresses and weakens considerably before reaching the opposite phase. The marked difference in the amplitudes makes the wave almost a standing wave. This PNA pattern is particularly sensitive to tropical forcing, as shown by Simmons (1982), and is recovered by Ferranti et al. (1990) through composite analysis keyed to the phases of the Madden and Jullian oscillation in the tropical OLR. There are definitely links between the two oscillations.

More surprising is the existence of a 30-35 day period exhibited in pair 3-4. Its composite evolution is displayed by sectors on Fig. 11. Note that there is almost no difference between this mode and the 50 day mode, except some poorly significant details over the Atlantic. Therefore, one suspects that this mode is due to large fluctuations in the period of a more general 30-60 oscillation. This explanation, however, is not fully satisfactory, since the result is robust to a change in the parameters of the method. Another consistent explanation would be that PNA responds to another type of forcing, such as the 30-35 day Atlantic oscillation. This hypothesis is however not really convincing either since so far, we have not been able to show phase relations between the two ATL and PAC 30-35 day oscillations. The third pair, 7-8 (not shown), has a shorter period (20-25 days), and closely resembles the Branstator-Kushnir retrogressing wave.

3.3 Results for the NH domain

The results of the experiments performed on the NH domain mostly confirm the previous results. With a window length of 200 days, The annual and semi-annual cycles are present in pairs 1-2 and 3-4. The PAC third harmonic disappears, but the 70 day Atlantic oscillation is found as pair 8-9, with a spatial structure strikingly similar to the one found for the ATL analysis. Then, faster 30-60 modes are found at higher orders. With the shorter window length, a dominant mode with a period of 40 days having the exact same structure as the one obtained by Kimoto *et al.* (1991), who used a different set of parameters. This mode resembles both the Atlantic and Pacific oscillations (not shown). Analysis of the phase relations between these modes show that there are significant links between them. The

amplitudes are bigger over the Atlantic than the Pacific, and weaker links are found with the Pacific modes than with the Atlantic modes. The problem of distinction between these oscillations remains open. The branstator-Kushnir wave is also explained in another higher-order pair.

Finally, we show on Fig. 12 all the composite trajectories, based on sector categories, projected on the plane spanned by s-EOFs 1 and 3 of the NH domain. Although far from being a correct phase-space portrait, this figure gives an idea about the location in phase space of possible unstable periodic orbits. Also shown on this projection is the likeliness of the NH 40 day oscillation to behave as the ATL 30-35 day oscillation, rather than the PAC oscillations. Some stability experiments were performed by taking the two halves of the data set, or by taking even or odd years. Also, analysis were conducted using different sampling rates, window lengths, or analysing only winter data. The same qualitative results hold, which confirms the statistical significance of the oscillations.

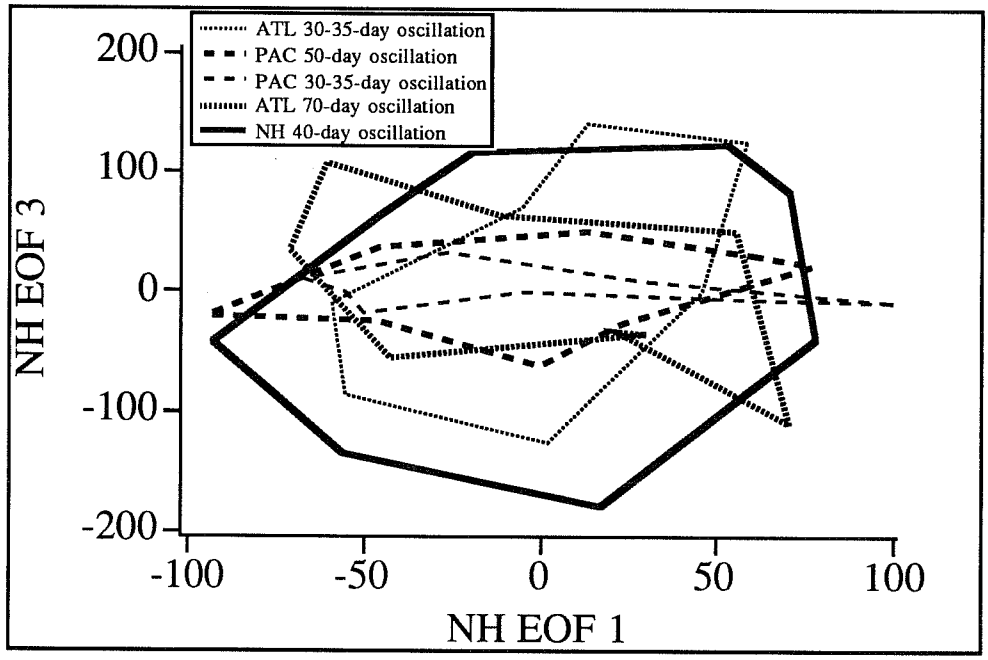

Fig. 12 Projection of the different composite evolutions in the space spanned by the NH s-EOFs 1 and 3. In this form of display, the composites shown on Figs. 7, 8, 10 and 11 are represented by a single point. Lines are drawn between successive sectors of the same composite.

3.4 Oscillations and Atlantic weather regimes

We address here the question whether oscillations can provide favourable environments for the occurrences of the weather regimes identified by Vautard (1990, see the Appendix for the dates). On Fig. 13a are displayed the events of the four Atlantic regimes BL, ZO, GA, and AR shown in Fig. 2, as pieces of the reconstruction of the ATL 70 day oscillation, under the

same projection as the one in Fig. 6. Clearly, BL events tend to happen more in sectors 2 and 3, ZO happens more in sectors 5 to 8, whereas AR and GA events do not seem to show preferred sectors of occurence.

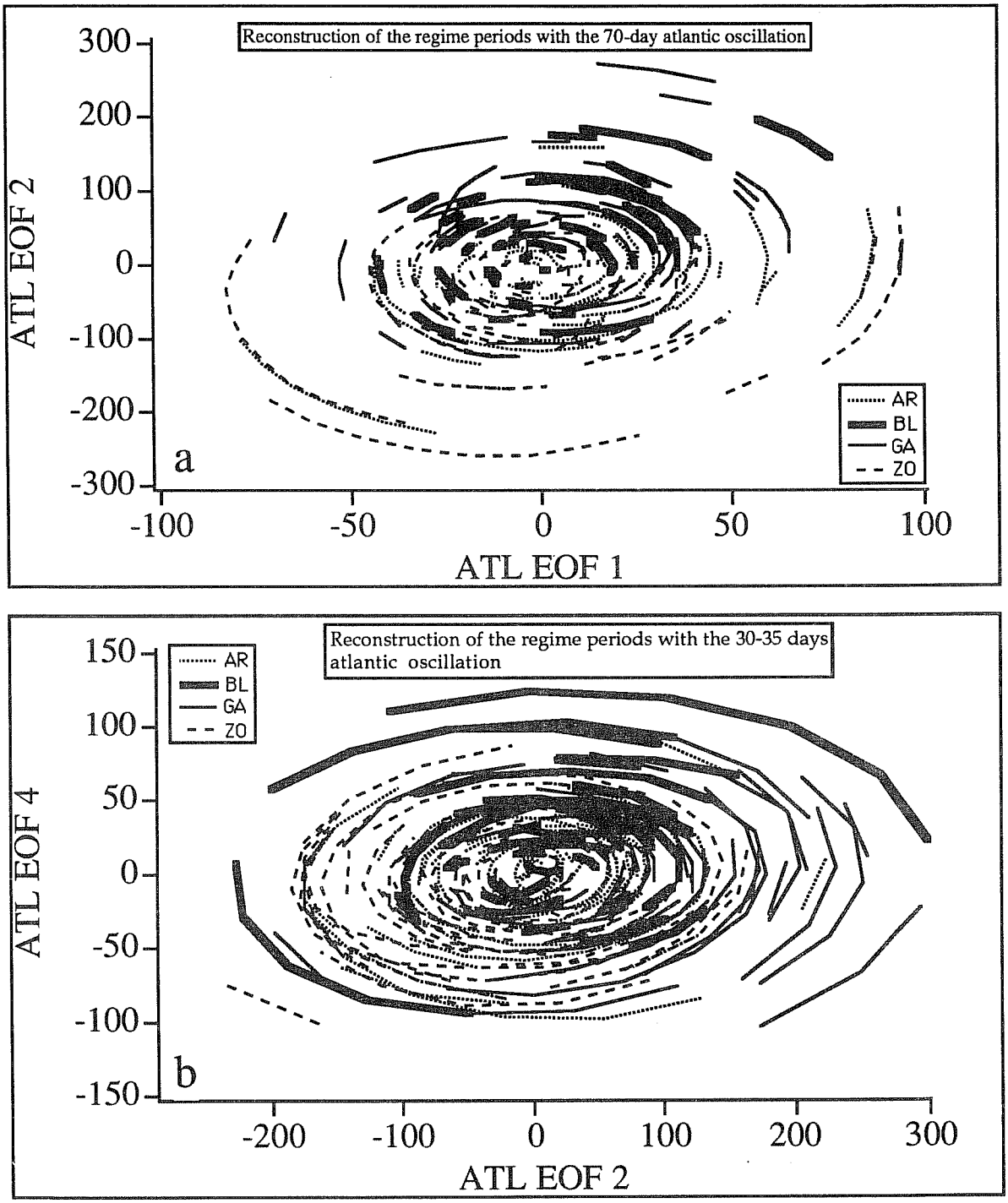

Fig. 13 Projection onto the ATL s-EOFs 1 and 2 (a), and 2 and 4 (b) of the reconstruction of the ATL 70 day oscillation (a) and ATL 30-35 day oscillation during regime events. Four line patterns correspond to the four different regimes displayed also on Fig. 2.

The preference of BL, ZO, and GA events is even more striking in the sectors of the ATL 30-35 day oscillation (Fig. 13b). The prefered transitions ZO -> BL -> GA mentioned in Vautard (1990) are recovered here as three phases of the oscillation. Note that in this figure, the trajectory turns clockwise, due to the choice of the coordinates. The regimes do not occur systematically in some phases of the oscillations, so that they are not simply, as it has been argued, slow phases of some Rossby waves.

The only interpretation of these figures is that ATL oscillations favour the development of weather regimes. This is, as stated in the introduction, an important property to take into account for long-range forecasting. A model which is not able to reproduce the LFOs will probably do a bad job in forecasting blocking. On the other hand, there are many occurences of the phase which do not lead to weather regimes, showing that successful long-range forecasts of blocking, for instance, do not depend *only* on the quality of the forecasts of the oscillations.

4. SUMMARY AND DISCUSSION

We have applied the multi-channel singular spectrum analysis (M-SSA) to a set of 32 years of 700 hPa geopotential height data. This new analysis technique gives a rather complete description of the regular phenomena in the low frequencies. The major advantage of using M-SSA rather than other analysis methods such as complex EOF analysis, or POPs, is that M-SSA is a multi-lag analysis of the variance, and therefore covers a wide range of time scales. M-SSA provides spatial-temporal filters able to localise, both in time and space, intermittent oscillations. Indices of phase and amplitude are also provided, which allow composite analysis.

In this study, we have focused the variability from a month to a year. Several oscillations are found within this range. After the annual cycle ands 2 of its harmonics, are found a 70 day mode associated with a poleward motion in the Atlantic jet region, and several modes with periods in the range 30-60 days, associated with variability in the entire hemisphere. At this faster time scale, when the analysis is restricted to the Atlantic domain, a dominant mode of 30-35 is found, associated with the retrogression of a quadrupole anomaly across the Atlantic. When the analysis is performed over the Pacifc domain, the dominant mode has a period of 50 days, as found for the Madden and Jullian oscillation in the equatorial angular momentum fluctuations. There are aparently no phase relations between the Pacific and the Atlantic oscillations. However, when the whole hemisphere is considered, we find a

mixed Atlantic-Pacific with an average period (40 days), indicating that still some interactions exist between the two basins. Although the problem remains to be clarified, there seems to be indications of two different mechanisms.

The question of the origin of these oscillations is a more difficult question. First, there are undoubtedly some links between the 30-60 day modes and the tropical Madden and Jullian oscillation, as shown by Kimoto *et al.* (1991). Since the response to tropical forcing in the Pacific is essentially a PNA pattern, the 50 day Pacific mode is probably partly coupled with the tropical oscillation. On the other hand, the large amplitudes over the Atlantic region for the 30-35 day mode have to be explained differently. There are good reasons to believe that the transients are playing an important role. First, it is now agreed that transients contribute crucially in the maintenance of the large-scale flow, as shown by a number of authors during the last decade. Second, free modes with such large-scale patterns are usually stable both baroclinically and barotropically. Third, the time scales involved in these low-frequency oscillations is much larger than the time scale involved for the development of baroclinic activity. Therefore, transients "have time" to act on average onto these patterns. If a proper scale separation is made, such as the one given by the reconstruction algorithm presented in Section 2, one could view the evolution equations of the oscillation as being schematically

$$\frac{dA}{dt} = F(A,A) + G(A), \qquad (4.1)$$

where A is a vector describing the oscillation, F(A,A) represents schematically the interaction of A with itself, and G(A) is the average feed-back of the transients onto the low-frequency oscillation. G(A) is in fact a term of parametrisation, which depends obviously on the large-scale configuration. Building such a model is the next step in the understanding of the fundamental mechanisms. Both the 70 day mode and the 30-35 day mode are likely to respond to transient feed-back, as proposed in Section 3.

The analysis of the relations between the oscillations and the weather regimes show important facts: the Atlantic weather regimes tend to occur in prefered phases of the two Atlantic oscillations. This indicates that certain phases of the oscillations act as favourable environments for the development of blocking or other regimes. This has an important consequence in forecasting : a necessary condition for GCMs to produce blocking and other regimes is that they reproduce well the oscillations. On the other hand, if one successful forecasts of the oscillations, does not necessarily imply successfull forecasts of the weather regimes.

M-SSA does not provide new directions of research only in the understanding of the mid-latitude circulation, but also is easily coupled with some linear forecasting methods, such as maximum entropy methods. Such an application of SSA has been investigated by Keppenne and Ghil (1991) who gave 30-month valid forecasts of the southern oscillation index. When applied to the short IPCC global surface temperature series, forecasts seem to remain valid up to a five years lead time (Vautard *et al.*, 1991). Thus, there is a hope that at least a nonnegligeable part of the variance, associated with the oscilations, may be forecasted easily by simple linear models. If the drift of the general circulation models in the long term distorts the parameters (frequency, amplitude) of these regular oscillations, it could be useful to consider the outputs of the simple linear empirical models as constraints on the GCMs to produce better long-term forecasts.

REFERENCES

Branstator, G., 1987: A striking example of the atmosphere's leading travelling pattern. *J. Atmos. Sci.*, **44**, 2310-2323.

Broomhead, D. S., and G. P. King, 1986: Extracting qualitative dynamics from experimental data. *Physica D* **20**, 217-236.

Charney, J.G., and J.G. DeVore, 1979: Multiple flow equilibria in the atmosphere and blocking. *J. Atmos. Sci.*, **36**, 1205-1216.

Colucci, S. J., 1985: Explosive cyclogenesis and large-scale circulation changes: implications for atmospheric blocking. *J. Atmos. Sci.*, **42**, 2701-2717.

Dickey, J. O., M. Ghil and S. L. Marcus, 1991: Extratropical aspects of the 30-60 day oscillation in the length-of day and atmospheric angular momentum. *J. Geophys. Res.*, in the press.

Ferranti, L., T. N. Palmer, F. Molteni, and E. Klinkler, 1990: Tropical-extratropical interaction associated with the 30-60 day oscillation and its impact on medium- and extended range predictability. *J. Atmos. Sci.*, **47**, 2177-2199.

Ghil, M., and K.C. Mo, 1991: Intraseasonal oscillations in the global atmosphere-Part I: Northern Hemisphere and Tropics, *J. Atmos. Sci.*, **48**, 752-779.

Hoskins, B. J., I. M. James and G. H. White,1983: The shape, propagation and mean-flow interaction of large-scale weather systems. *J. Atmos. Sci.*, **40**, 1595-1612.

Itoh, H., 1985: The role of transient motions in the formation of quasi-stationary planetary waves. *J. Atmos. Sci.*, **42**, 917-932.

Keppenne, C. L., and M. Ghil, 1991: Adaptative spectral analysis and prediction of the Southern Oscillation Index, in Proc. 15th Annual Climate Diagnostics Workshop, U.S. Dept. of Commerce, NOAA/Climate Analysis Center (1991); also Adaptative spectral analysis, and prediction of the Southern Oscillation Index, *J. Geophys. Res.*, submitted.

Kimoto, M., M. Ghil and K.C Mo, 1991: Spatial structure of the extratropical 40 day oscillation, in preprints Eight Conference on Atmospheric and Oceanic Waves and Stability (in press).

Kushnir, Y., 1987: Retrograding wintertime low-frequency disturbances over the North Pacific Ocean. *J. Atmos. Sci.*, **44**, 2727-2742.

Legras, B. and M. Ghil, 1985: Persistent anomalies, blocking, and variations in atmospheric predictability. *J. Atmos. Sci.*, **42**, 433-471.

Lorenz, E. N., 1963: Deterministic nonperiodic flow. *J. Atmos. Sci.*, **20**, 130-141.

Madden, R. A., and P.R. Julian, 1971: Detection of a 40-50 day oscillation in the zonal wind in the tropical Pacific, *J. Atmos. Sci.*, **28**, 702-708.

Mullen, S. L., 1987: Transient eddy forcing of blocking flows.*J. Atmos. Sci.*, **44**, 3-22.

Pike, E. R., J.G. McWhirter, M. Bertero and C. de Mol, 1984: Generalized information theory for inverse problems in signal processing, IEEE Proc. **131**, 660-667.

Penland, M. C., M. Ghil and K. Weickmann, 1991: Adaptative filtering and maximum entropy spectra with application to changes in atmospheric angular momentum, *J. Geophys. Res.*, in the press.

Plaut, G., and R. Vautard, 1991: Spells of oscillations in the atmospheric low-frequency dynamics of the Northern Hemisphere, in preparation.

Preisendorfer, R. W., 1988: Principal Component Analysis in Meteorology and Oceanography (C.D. Mobley, ed, Elsevier, Amsterdam, 1988).

Rasmusson, E. M., X. Wang and C.F. Ropelewski, 1990: The biennial component of ENSO variability, *J. Mar. Syst.*, **1**, 71-96.

Rex, D.F., 1950: Blocking action in the middle troposphere and its effect on regional climate. Part I: An aerological study of blocking action. *Tellus*, **2**, 196-211.

Shutts, H. G. J., 1983: The propagation of eddies in diffluent jet streams: eddy vorticity forcing of "blocking" flow fields. *Quart. J. Roy. Met. Soc.*, **109**, 737-761.

Simmons, A. J., 1982: The forcing of stationary wave motion by tropical diabatic heating. *Quart. J. Roy. Meteor. Soc.*, **108**, 503-534.

Vautard, R., and B. Legras, 1988: On the source of midlatitude low-frequency variability. Part II: Nonlinear equilibration of weather regimes. *J. Atmos. Sci.*, **45**, 2845-2867.

Vautard, R., and M. Ghil, 1989: Singular spectrum analysis in nonlinear dynamics with applications to paleoclimatic time series, *Physica D* **35**, 395-424.

Vautard, R., 1990: Multiple weather regimes over the north Atlantic. Analysis of precursors and successors. *Mon. Wea. Rev.*, **118** (10), 2056-2081.

Vautard, R., P. Yiou, and M. Ghil, 1991: Singular spectrum analysis: a toolkit for noisy chaotic signals, submitted to Physica D.

Wallace, J. M., and D. S. Gutzler, 1981: Teleconnection in the geopotential height field during the northern hemisphere winter. *Mon. Wea. Rev.*, **109**, 784-812.

Weare, B. C., and J.N. Nasstrom, 1982: Examples of extended empirical orthogonal function analyses, *Mon. Wea. Rev.*, **110**, 481-485.

Weickmann, K. M., 1983: Intraseasonal circulation and outgoing longwave radiation modes during northern hemisphere winter. *Mon. Wea. Rev.*, **111**, 1838-1858.